Colloids and Surfaces A 537 (2018) 185–196

Contents lists available at ScienceDirect

Colloids and Surfaces A

journal homepage: www.elsevier.com/locate/colsurfa

Research Paper

Fabrication of folic acid magnetic nanotheranostics: An insight on the formation mechanism, physicochemical properties and stability in simulated physiological media

Pamela Azcona, Ignacio López-Corral, Verónica Lassalle*

INQUISUR-UNS-CONICET, Avda. Alem 1253, 8000, B. Blanca, Bs As, Argentina

GRAPHICAL ABSTRACT

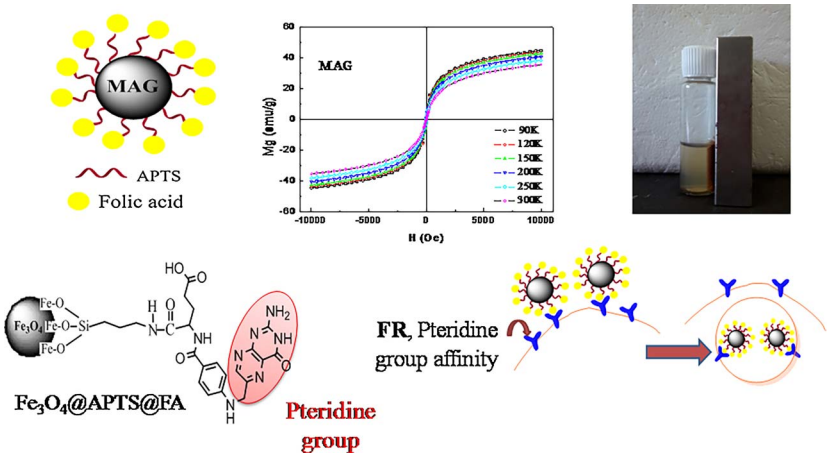

ARTICLE INFO

Keywords:
Magnetic nanoparticles
Theranostics
Folic acid
Simple adsorption
Covalent linkage
Bovine serum albumin

ABSTRACT

Nanodevices based on magnetite functionalized with folic acid (FA) with improved properties to be employed as theranostics in various types of cancer are here proposed. Two methodologies for FA incorporation were explored aiming to reach suitable loading efficiency as well as adequate stability of nanosystems in physiological media. To this end, simple adsorption and covalent binding of FA and some experimental conditions derived from both procedures were studied. A thorough physicochemical characterization was performed using all the formulations. The mechanism of the interaction between FA and magnetite nanoparticles (MNPs) was elucidated from characterization results supported by theoretical studies using spin-polarized density functional theory (DFT). Both data coincide in that the selective functional group of FA (pteridine group) remained available after FA binding MNPs. Such studies also demonstrated that any of FA carboxylate groups could be available to potentially link other molecule (i.e therapeutic agents). Besides, other issues that are not normally accomplished in reported articles were included; i.e the stability according to two different criteria: size evolution (expressed as hydrodynamic diameter) as a function of time in aqueous media; and the capacity FA retention in PBS, pH = 7.4. Recovered data indicated that the samples are stable at least 15 days in water and 4 h in buffer without significant modifications of their properties. The feasibility of these formulations to interact with simulated physiological fluid was also assayed. The results revealed that protein corona was formed around all the tested formulations leading to more stable nanodevices in terms of their hydrodynamic sizes and size evolution

* Corresponding author.
E-mail address: veronica.lassalle@uns.edu.ar (V. Lassalle).

http://dx.doi.org/10.1016/j.colsurfa.2017.10.025
Received 3 July 2017; Received in revised form 5 October 2017; Accepted 8 October 2017
Available online 09 October 2017

along the time. To complete the theranostic characteristic, Doxorubicin was added to the MNPs@FA by physical adsorption, to provide the therapeutic function. The satisfactory incorporation was verified by FTIR spectroscopy.

1. Introduction

With the advance of nanotechnology, a large variety of nanocarriers has been optimized in terms of their in vivo performance and their ability to reach specific sick regions in the body. In this regards multifunctional nanosystems have emerged providing both inputs: therapeutic and diagnostic in an unique device, actually known as theranostics [1,2]. In this concern, it is possible to combine therapeutic strategies such as nucleic acid delivery, chemotherapy or hyperthermia with one or more imaging functionalities, such as magnetic resonance imaging (MRI), for both, in vitro and in vivo, studies. Moreover, with the implementation of this type of technology it would be possible to obtain information not only of an initial diagnosis, but also theranostics would serve for monitoring the progress of the pathology in real time, giving light on the efficiency of a medical treatment [3,4]. Currently, the most studied pathologies regarding the application of theranostics are oncological diseases because of their social impact and the benefits offered by these novel technologies [5–8]. Magnetic nanoparticles based on iron oxides (MNPs), i.e magnetite (Fe_3O_4) and maghemite (γ-Fe_2O_3), have been of great interest in several nanomedicine fields. They have been successfully employed in MRI and hyperthermia treatments due to their magnetism (or superparamagnetism), biodegradability and relatively low toxicity [9,10]. In spite of the wide information regarding to biomedical applications of MNPs, their practical implementation has not been concreted yet. In fact, only a few iron oxide based nanosystems are currently available in the market [11] and any of them is devoted to therapeutic non theranostics issues. This inconsistence is, in part, because MNPs may accumulate at reticuloendothelial sites such as the liver, spleen and kidney. In consequence, insufficient uptake at tumor sites would decrease the therapeutic benefits of the administrated drug dose, and non-specific association with healthy tissues would lead to toxic side effects. This limitation prevents drug-loaded nanoparticles from achieving the potential therapeutic effects they might otherwise attain.

A recent strategy to achieve efficient tumor targeting is to conjugate drug carriers with specific ligands able to recognize molecular receptors on the surface of cancer cells. Among different targeting ligands, folic acid (FA), represents an attractive option to modify MNPs because it is a low cost, biocompatible, and non inmunogenic molecule. Moreover, FA is of high importance for the synthesis of new cells since it is necessary for the biosynthesis of DNA bases. Because of this, FA receptors (FR) with high affinity are overexpressed in several types of cancer cells [12]. Nanocarriers conjugated with FA may be targeted to tumor cells and internalized through receptor-mediated endocytosis.

Although abundant works may be found in open literature devoted to the preparation of FA modified Fe_3O_4 MNPs because of the abovementioned issues [13,14], some aspects related to the interaction mechanisms as well as the stability of the prepared nanosystems are missing. It is important to highlight that those aspects are crucial to the in vivo implementation of FA-based systems.

Different pathways have been reported to achieve nanocarriers conjugated FA. From them, the most widely used protocol involves a covalent linkage with, generally, an aminated nanoparticle's surface. For example, Huang et al. designed a nanoplatform for delivery of drugs based on polymers coated SPIONs modified with FA. In such work, the nanoparticles obtained by thermal decomposition of $Fe(acac)_3$, were functionalized directly with FA employed dimethylsulfoxide (DMSO), 3-(3-dimethylaminopropyl)-1-ethylcarbodiimide hydrochloride(EDC) and *N*-hydroxysulfosuccinimide sodium salt (sulfo-NHS) in only one step. Polyethilene imine (PEI) was the source of amino groups to conjugate with FA [13]. On the other hand, Yang et al., functionalized nanoparticles of chitosan with FA using the same reagents for carrying 5-aminolaevulinic acid (5-ALA) and to determine its targeting and uptake efficiency in different human colorectal cancer cell lines (HT29 and Caco-2) by folate receptor-mediated endocytosis [14]. Patel et al. prepared core-shell hybrid iron oxide-zinc oxide nanoparticles conjugated folic acid for applications as a photosensitier (PS) in photodynamic therapy. In this case, they first conjugated FA with *N*-hydroxysuccinimide (NHS) and then the product reacted with amino group from the nanocarriers cover with tetraethylorthosilicate (TEOS) and (3-aminopropyl)triethoxysilane (APTS) [15].

The aim of this contribution is to prepare MNPs modified with folic acid with improved properties to be employed as theranostics to the treatment and diagnostic of various types of cancer. To do this, an initial in deep study is presented devoted to find an efficient incorporation procedure for the FA molecules to the MNPs surface. It is important to remark that even when vast information about these methods may be found in open literature, the most of them include a large number of reactants without a clear justification on the role of each one on the nanocarriers structure. Here we intend to simplify the procedure by employing the minimum amount of steps and reactants to link FA on the MNPs surface.

The focus was not only on achieving high levels of loaded FA, but mainly in reaching a stable formulation able to retain the FA as well as their physicochemical properties. The mechanism of MNPs@FA interactions is studied aiming to elucidate if the potentially selective functional groups remained surface exposed. To develop this issue experimental data and computational tools have been combined. The behaviour of MNPs@FA in a media simulating the blood plasma is also presented as an initial stage to assess the viability of these nanosystems. Size, aggregation trend and stability were the analyzed parameters.

Besides, preliminary results regarding to the incorporation of an oncological drug, Doxorubicin, are also presented. On this way, this research may be considered as a necessary prior study to the design of a nanoplataform susceptible of being in vivo assayed.

2. Materials and methods

2.1. Materials

All reagents and solvents were of analytical grade and used without further purification. Ferric chloride hexahydrate (99.99%) and sodium dodecyl sulfate (SDS) was provided by Biopack (Argentina). Ferrous sulphate heptahydrate (99.99%) was provided by Mallinckradt Chemical Works (USA). Sodium hydroxide and acetic acid (AA) (28–29%) were purchased from Cicarelli (Argentina). Absolute ethanol was provided by Quimicor (Argentina). (3-aminopropyl)triethoxysilane (APTS) was provided byAvocado Research chemicals (United Kingdom). *N*,*N*′-diciclohexilcarbodiimida (DCC) was purchased from Fluka (Germany). Folic acid (FA), dimethylsulfoxid (DMSO) and Doxorubicin hydrochloride (Doxo) were purchased from Sigma Aldrich (Germany). Bovine serum albumin (BSA) was provided by Winer Lab, and Ringer Solution (RS) was obtained from ROUX-OCEFA S.A (Argentina). Distilled water with conductivity about 5.00 μS was employed.

2.2. Methods

2.2.1. Synthesis of MNPs

Magnetite nanoparticles (MNPs) were synthesized by co-

precipitation with a series of simple modifications to the traditional methodology [16]. Briefly, an aqueous solution of $FeCl_3{\cdot}6H_2O$ and $FeSO_4{\cdot}7H_2O$ (ratio2/1), containing 0.0027 mol of SDS was prepared. This mixture was added to an alkali solution of NaOH 5 M in a controlled way. The described procedure was carried out at room temperature (r.t) and in presence of visible light, generated by a tungsten

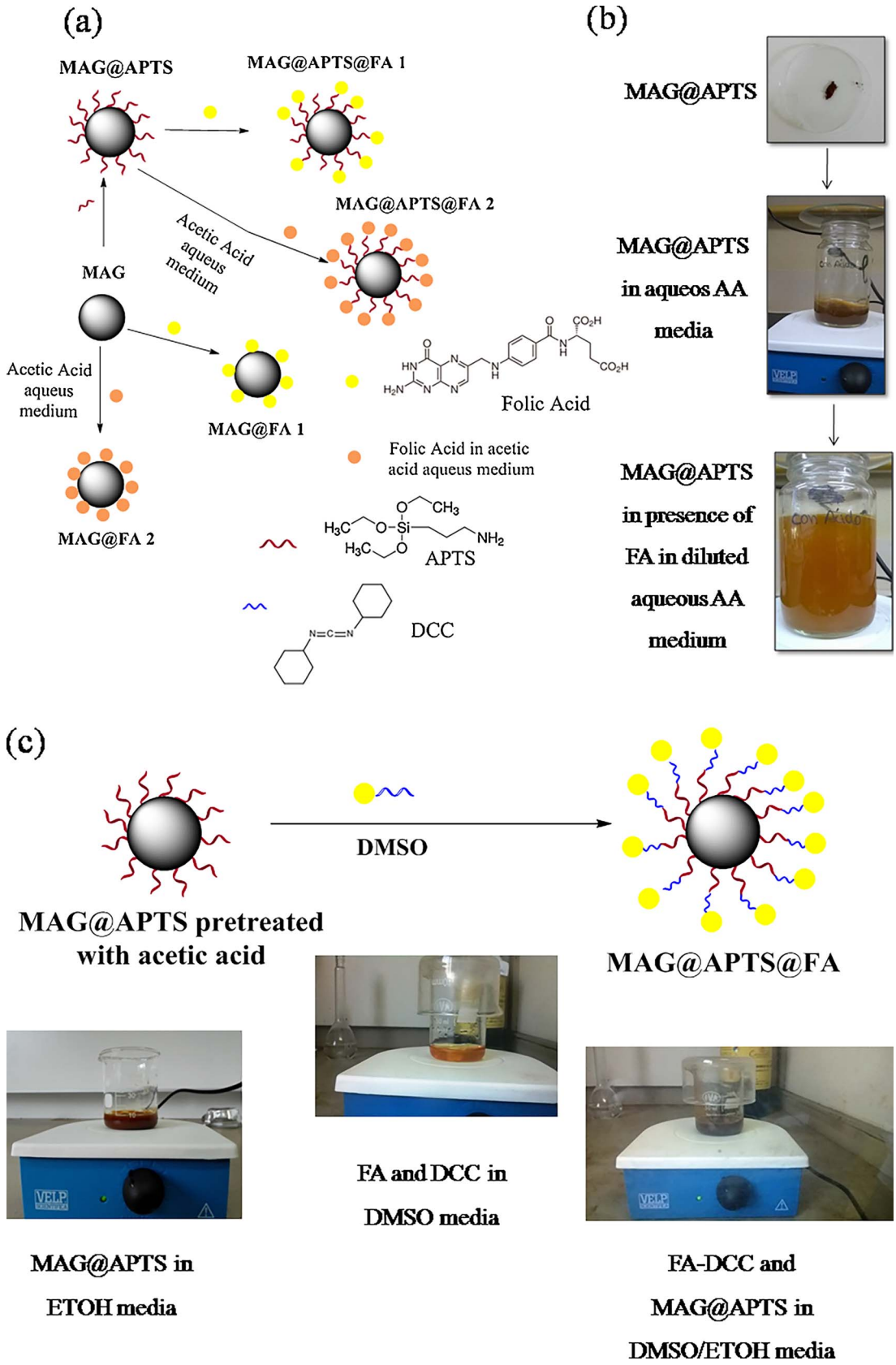

Scheme 1. Incorporation of folic acid to MNPs'surface. (a) Simple adsorption. (b) Images of the simple adsorption process. (c) Images and scheme of covalent linkage method.

lamp. After this process, a dark solution was obtained and decanted using a magnet. The supernatant was extracted, and the solid was washed several times with distilled water and eventually ethanol. Washings were repeated until pH and conductivity reached the levels corresponding to distilled water. The solid obtained after dry in oven at 45 °C overnight under vacuum was called MAG.

2.2.2. Modification with APTS

Treatment with APTS was necessary to provide to MNPs the suitable functional groups to interact with FA. In brief, 3.01×10^{-3} moles of APTS were added to 1.17×10^{-3} moles of MAG in 75 mL of absolute ethanol and stirred vigorously for 8 h. The solution was decanted using a Nd magnet and washed several times with absolute ethanol to eliminate the APTS excess. The sample was called MAG@APTS.

2.2.3. Incorporation of folic acid to MNPs

2.2.3.1. Physical adsorption. In brief, MAG or MAG@APTS were treated with an aqueous solution of acetic acid (AA) and stirred for 30 min at r.t. Then, 20 mg of FA were added with distillated water to reach a final volume of 100 mL and the reaction was allowed during 24 h (See Scheme 1a and b). The obtained samples were named: MAG@FA 1, MAG@FA 2, MAG@APTS@FA 1 and MAG@APTS@FA 2. The number 1 involves synthesis in absence of AA and 2 synthesis in presence of AA. Table 1 includes the explored experimental conditions.

2.2.3.2. Covalent link. Through this procedure, the goal was to induce a covalent linkage MNPs@FA through carboiimide (DCC) intermediate reaction. Methodology was adopted from reported article by Jiang et al. with some modifications [17]. Briefly, 100 mg of FA and 36 mg of DCC were dissolved in 5 mL DMSO and stirred during 30 min at r.t. After this, 5 mL of a dispersion containing 100 mg of MAG@APTS in ethanol was added. The reaction was allowed for 24 h at r.t under magnetic stirring (See Scheme 1c). At the end, the obtained product was washed to remove the side-product formed by insoluble dicyclohexylurea (DCU) aggregates and the residues of DMSO. To do that, the sample was dispersed in water and buffer PBS, pH = 7.4, shaken vigorously 30 min under magnetic stirring and decanted using an Nd magnet. This procedure was repeated until the insoluble DCU moieties at the surface of supernatant were completely removed.

The obtained products were named E1, E2 and E3 following the same protocol with some experimental variants, as may be seen in Table 1.

2.3. Characterization

Transmission Infrared Fourier Transform Spectroscopy (FTIR) was performed using a Thermo Scientific Nicolet iS50 NIR module with Integrating Sphere in the frequency range 4000–400 cm^{-1}. A few milligrams of the samples (10–20 mg) were mixed in a mortar manually with ~50 mg of KBr dry powder. The mixture was compacted and placed in the sample unit of the FTIR spectrometer.

UV–vis spectroscopic measurements were carried out using a spectrophotometer Shimadzu 160 Japan. Dispersion of different formulations of (1 mg of nanoparticles/25 mL of bidistilled water), were ultrasonicated during 60 min and employed by analyzing the absorbance at 280 nm [18].

Transmission electron microscopy (TEM, JEOL 100 CX II, Tokyo, Japan) were used to examine the morphology and estimate the size of the nanoparticles. The TEM samples were dispersed in distilled water or ethanol, placed on 200 mesh Cu grids and dried at r.t.

Thermogravimetric analyses (TGA) were performed using a Rigaku DTA-TAS 1000 equipment. Different masses of magnetic formulations were weighted and heated from r.t to 500 °C at a rate of 10 °C/min under air atmosphere.

Atomic absorption spectroscopy was implemented to evaluate the composition of the nanoparticles in terms of total iron content. For these measurements, 10 mg of different magnetic formulations were dissolved in 25 mL of HCl 10% w/v and measured in a GBC Avanta 932.

Malvern Zetasizer was used to measure the Z potential (ζ) and the hydrodynamic average particle diameter (HD, nm). Aqueous dispersions of samples were prepared at a concentration of 0.1 mg of nanoparticles/mL. In the case of HD the samples were ultrasonicated during 60 min previously to the assay. The informed values were an average of about five-seven repeated measurements.

2.4. Density functional theory calculations

Quantum-chemical calculations were performed in order to compare stability of the different MAG@APTS@FA systems that could be obtained. In order to simplify the model and avoid unnecessary details and consequent longer calculation time, we assumed that the APTS-FA interactions are only slightly affected by the nanoparticle presence, so the single APTS@FA moiety has been modeled. The calculations were carried out in the framework of spin-polarized density functional theory (DFT), using the SIESTA (Spanish Initiative for Electronic Simulations with Thousands of Atoms) code [19,20]. We selected the generalized gradient approximation functional parameterized by Perdew, Burke and Ernzerhof (GGA-PBE) [21]. A double-ζ plus polarization (DZP) basis sets for the valence electrons [20,22] was chosen. The core electrons were modeled by standard norm-conserving Troullier-Martins pseudopotentials [23]. A cutoff of 150 Ry for the grid integration was used to represent the charge density [19]. Full geometry optimizations without symmetry constraints were performed with the conjugate gradient (CG) minimization scheme until the forces on each atom were less than 0.04 eV/Å.Once the equilibrium geometries were obtained, we computed the overlap population (OP) belonging to selected atom pairs. The OP value constitutes a measure of the bonding between two atoms [24].

Table 1
Different formulations of MNPs@FA as a function of experimental conditions used to promote FA linkage.

Sample	FA Concentration (mg/mL)	Nominal Ratio MAG/FA (w/w)	Additives
MAG@FA 1	0.21	1/1	–
MAG@FA 2	0.21	1/1	Acetic Acid [C] = 1.6 mol/L
MAG@APTS@FA 1	0.21	1/1	–
MAG@APTS@FA 2	0.21	1/1	Acetic Acid [C] = 1.6 mol/L
E1	6.7	2/1	Acetic Acid [C] = 1.6 mol/L DCC = 7.2 mg/mL DMSO DMSO = 2.5 mL
E2	10	1/1	Acetic Acid [C] = 1.6 mol/L DCC = 7.2 mg/mL DMSO DMSO = 5 mL
E3	13.3	1/2	Acetic Acid [C] = 1.6 mol/L DCC = 7.2 mg/mL DMSO DMSO = 10 mL

2.5. Stability assays

2.5.1. Evolution of hydrodynamic diameter as a function of time

The evolution of hydrodynamic diameter as a function of the time was achieved to evaluate the stability of different formulations. In this regards, dispersions of different samples were prepared in distilled water and sonicated during 60 min previous to measure the average hydrodynamic diameter. The measurements were performed once a week during one month employing the original dispersion. After this period of time the solid was tested for the FA retention using FTIR spectroscopy.

2.5.2. Stability assays in phosphate buffer saline

Further assays were performed aiming to monitor the permanence of FA on the MAG@APTS surface. To do this, E1, E2 and E3 were incubated in buffer phosphate, pH 7.4 (PBS) during 4 h at r.t under magnetic stirring. Finally, the obtained suspensions were decanted using a magnet and the supernatants were extracted. FTIR assays were performed on the solids to verify the presence of FA on the MAG@APTS surface.

2.6. Interactions with plasmatic components

An incubation of MAG@APTS and E2 with a media simulating the biological one was implemented in order to study the way of these formulations interact with biological fluids. Bovine serum albumin (BSA) was used as predominant protein in physiological fluid (as analogous of human serum albumin) whereas the media was Ringer Solution. This solution was chosen since it has the same osmolarity and electrolytic concentration to blood. pH was adjusted to 7.4. This media will be named simulated physiological fluid (SPF) here in after. Briefly, 50 mg of E2 were incubated in 250 mL of SPF at 37 °C containing 1125 mg of BSA during 4 h. In addition, E2 behavior in SPF media without BSA was also examined, with two different ends: by one side, to evaluate the possible FA lost during incubation. By the other side, this assay was taken as control of BSA.The same procedure was followed using MAG@APTS.

2.7. Loading of therapeutic agent

The incorporation of Doxorubicin (Doxo) was performed following the methodology reported by Sadighiana et al. with some modifications [25]. Briefly, 10 mg of E2 were mixed with 1 mg of Doxo in 1 mL of distillated water, for 24 h at r.t. The magnetic particles loaded Doxo were decanted using an Nd magnet. Sample was called E2@Doxo.

3. Results and discussion

3.1. Characterization of nanoparticles modified with FA

FTIR data was useful to confirm the coating with APTS and the further FA incorporation on MAG surface. Fig. 1a shows the spectrum of pure FA, where the typical bands at 3550 and 3400 cm^{-1} due to the hydroxyl (OH) stretching of glutamic acid and −NH groups may be observed. The peak associated to stretching vibration of C═O appears at nearly 1699 cm^{-1}, while the band at 1610 cm^{-1} may be related to the bending mode of NH− vibration. The signals appearing between 1500 and 1400 cm^{-1} may be attributed to absorption of the phenyl and

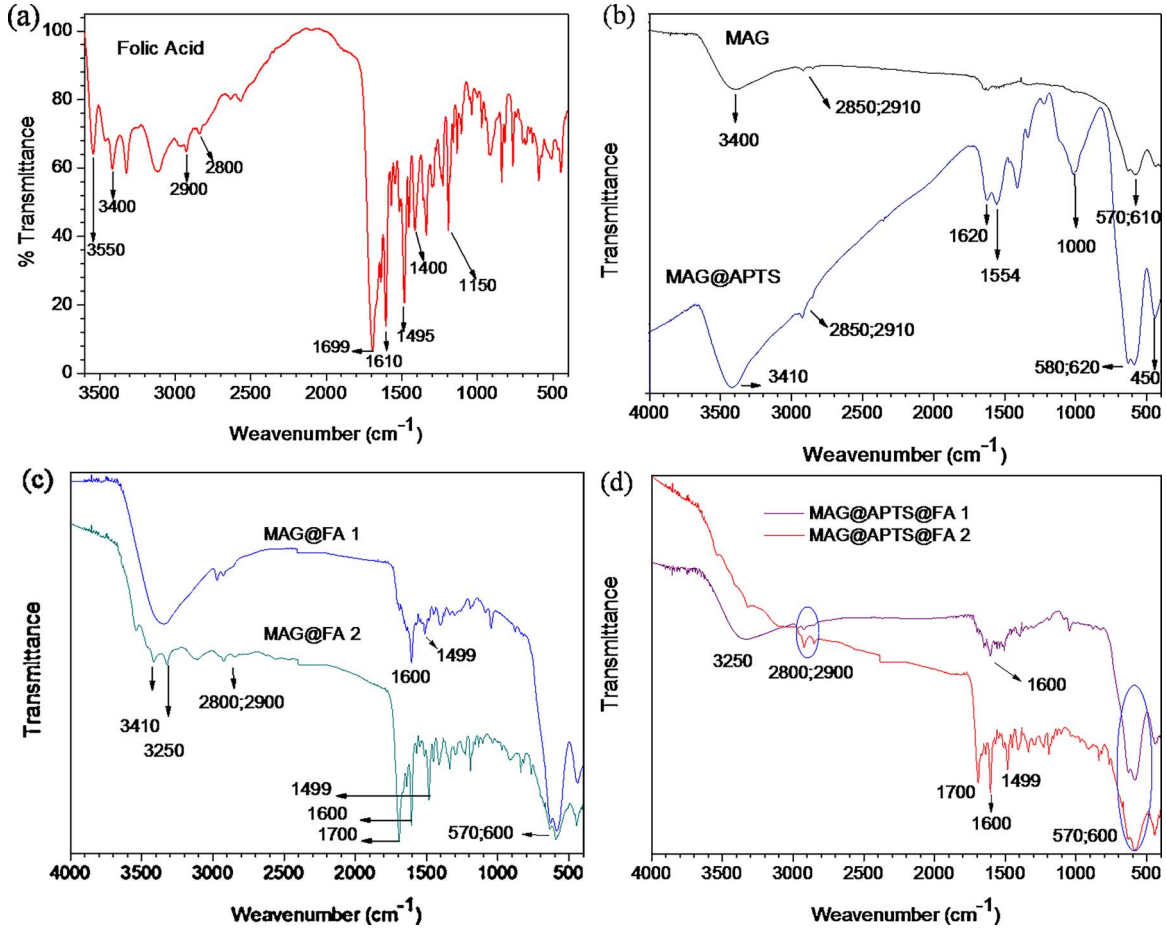

Fig. 1. (a) FTIR spectrum of Folic Acid. (b) FTIR spectra of MAG and MAG@APTS. (c) FTIR spectra of different MAG@FA samples obtained by simple adsorption. (d) FTIR spectra of MAG@APTS@FA samples obtained by simple adsorption.

pteridine ring (PT) [26]. The main objective in coating MAG with APTS was related to the possibility to improve the interactions with FA though APTS functional groups [27]. Fig. 1b shows the spectra corresponding to the MAG before and after APTS coating. The bands of APTS are clearly visualized at 2910 and 2850 cm^{-1} assigned to stretching vibration of C—H bond of the propyl amine group. The silica network adheres to the particle surface via Fe—O—Si bond. The absorption bands of the Fe—O bond of MAG shift from 570 and 610 cm^{-1} to 580 and 620 cm^{-1} in MAG@APTS. This could be justified in terms of the interactions Fe—O—Si [28]. Moreover, band around 1000 cm^{-1} from the Si—O—Si groups, confirmed the presence of the silane over the surface of MAG@APTS. The two bands at 1620 and 3410 cm^{-1} may be attributed to the N—H stretching vibrations and bending mode of free $-NH_2$ group, respectively. In addition, the presence of the peak at 1554 cm^{-1} may be ascribed to the deformation modes of the free amino groups [29,30].

From Fig. 1c and d, it is evident that the successful incorporation of FA on MAG nanoparticles was achieved by simple adsorption. The characteristic band of Si—O from the APTS is absent in spectra of almost all the samples. Moreover, typical bands from FA at 3500–3250 cm^{-1}, and 1700, 1600 and 1499 cm^{-1}, may be distinguished in the spectra of MAG@FA 2 and MAG@APTS@FA 2. Those may be ascribed to C═O and N—H functional groups.

As a difference, in the spectra of MAG@FA 1 and MAG@APTS@FA 1 only the band at 1600 cm^{-1} could be observed, suggesting that the presence of acetic acid in the media of reaction is crucial for the satisfactory FA adsorption. This result may be attributed to the occurrence of electrostatic interactions between amino from APTS and FA groups induced by the low pH [14].

The covalent coupling of FA was performed to reach a more stable formulation in terms of the retention of the acid on MAG@APTS along the storage time. It was performed via carboiimide linkage using DCC as coupling agent. FTIR spectra of E1, E2 and E3 are compared in Fig. 2a. The representative bands related to peptide bonds at 1691 and 1625 cm^{-1} may be distinguished in E1 to E3. These may be ascribed to flexion vibration of C═O and stretching vibration of N—C═O, respectively. Such signals are able to confirm the covalent FA linkage. The signals associated to DCC are missing. This is consistent with the mechanism of action of DCC as enhancer of electrophilicity of the carboxylated FA group [31].

Besides, the presence of FA was further confirmed by UV–vis spectroscopy. Fig. 2b shows the spectrum of a Folic Acid solution; where a signal a 280 nm ascribed to the $\pi \rightarrow \pi^*$ transition of PT ring is clearly observed [32]. In Fig. 2c UV spectra of MAG@APTS, E1, E2 and E3 are compared. It is possible to find a signal at 283 nm in E1, E2 and E3 spectra that is absent in MAG@APTS's spectrum. These semi-quantitative results are useful to demonstrate the slight differences in MNPs formulations prepared from different nominal FA amounts.

It is worth mention that both spectroscopic techniques coincide in demonstrating the satisfactory surface incorporation of FA.

Data regarding to hydrodynamic diameters and Z potential of all prepared formulations are included in Table 2. These results suggest that a slight increment of HD occurred after MAG coating with both, APTS and FA. Other researchers promoting the FA coupling or adsorption in different kind of supports have reported similar findings. For instance, Yang et al. prepared chitosan-FA nanoparticles as carriers to antitumoral delivery. They found that the average diameter of the prepared nanoparticles did not vary significantly with the incorporation of folic acid on chitosan polymer [14]. Therefore, the HD seems not to be sensible enough to FA incorporation.

Besides, the reached sizes are even suitable for in vivo administration according to previous own works [33,34].

As a difference, the FA and the proportion of this ligand affect the nanoparticles surface charge as demonstrate the Z potential data. Great variations in these results reveal the sequential incorporation of APTS and FA. In fact, positive ζ was measured in the case of MAG@APTS, due to the exposed protonated amine groups at fixed pH of distilled water (pH 5.7). The physical FA adsorption on bare MAG@APTS nanoparticles leads to a decrease of ζ (see MAG@APTS@FA in Table 2).

When the covalent linkage of FA is promoted, the ζ reaches high magnitude values but with negative sign. It is worth noting that this trend seems not to be affected by the initial concentration of FA. Similar trend was evidenced in other works, indicating that FA would expose negatively charged moieties reducing the Z potential value [14,35].

The incorporation of FA did not produce noticeable changes in terms of the morphology of the MNPs. The Fig. 3 includes TEM

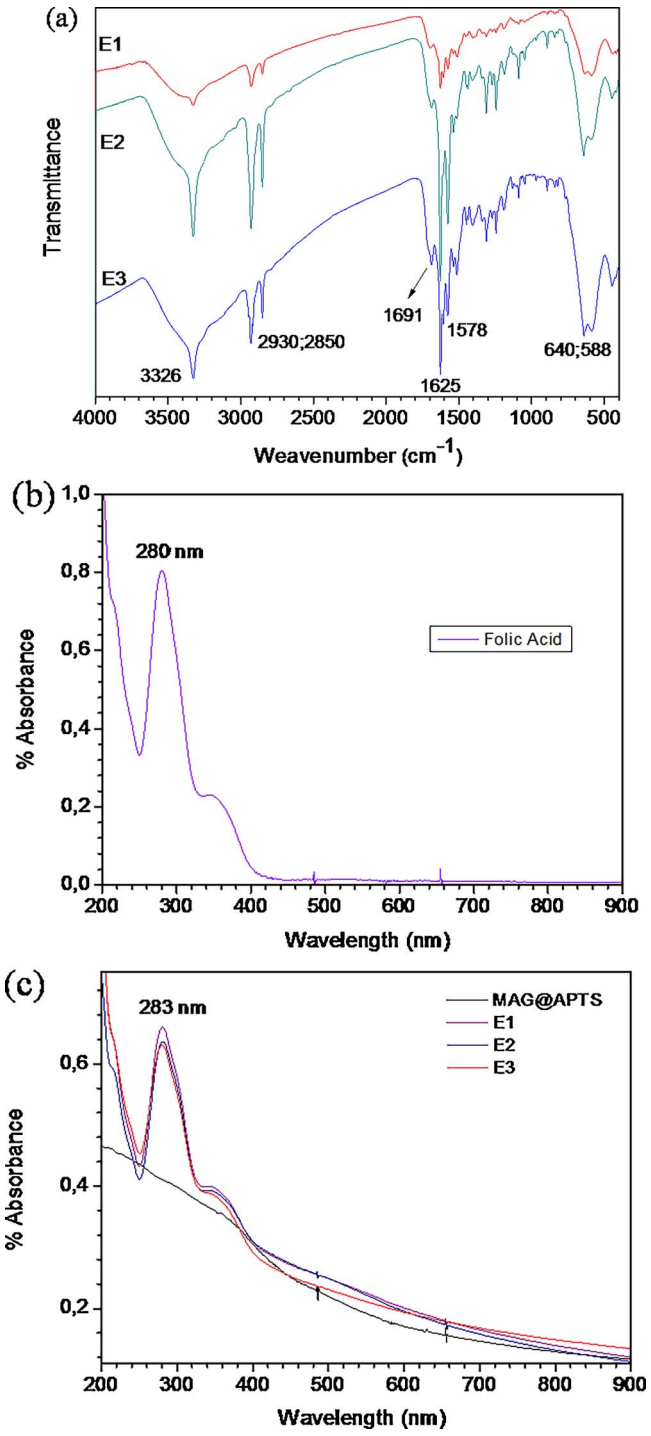

Fig. 2. (a) FTIR spectrum of MNPs modified with FA obtained by covalent linkage. (b) UV–vis spectrum of Folic Acid solution. (c) UV–vis spectra of MAG@APTS and E dispersions.

Table 2
Data on average hydrodynamic diameter and ζ of all the prepared formulations.

Sample	Average Hydrodynamic Diameter (nm)	ζ(mV), pH:5.7
MAG	254.6 ± 9.8 PDI: 0.245 ± 0.030	−25.1 ± 1.6
MAG@APTS	357.0 ± 8.2 PDI: 0.339 ± 0.025	31.8 ± 1.4
MAG@APTS@FA	451.6 ± 10.3 PDI: 0.326 ± 0.048	−10.6 ± 2.5
E1	364.2 ± 10.0 PDI: 0.388 ± 0.084	−16.3 ± 0.7
E2	342.1 ± 6.7 PDI: 0.318 ± 0.019	−22.0 ± 0.7
E3	381.2 ± 23.8 PDI: 0.487 ± 0.110	−23.4 ± 0.3

micrographies of raw MAG nanoparticles, MAG@APTS and E2, as example. It is clearly observed that the rod shape persisted even after the treatments performed to promote the FA linkage.

The stability of the samples E1, E2 and E3 was evaluated in terms of the evolution of their HD, measured in aqueous media, along the time. The results indicated that E1 could be storage as an aqueous dispersion at least 15 days without significant alterations in its HD, while E2 and E3 maintain their hydrodynamic sizes only along 7 days with slight modifications in identical conditions (data not shown included in Supplementary material (a)).

The Fig. 4 presents the thermograms of MAG@APTS and the corresponding to formulations containing FA covalently linked. It could be seen that all the samples experiment a mass drop caused essentially by water loss. Moreover, it may appreciate a weight drop of already 4% between 280 and 320 °C in the thermogram of MAG@APTS, revealing the thermal decomposition of the organic aminopropyl groups [30]. On the other hand, E1, E2 and E3 ‘s thermograms show two mass drop, between 230 and 410 °C, that may be ascribed to APTS and Folic Acid moieties loss, respectively. From these data, it may infer that the loss of organic compounds ranged between 11 and 41% in almost all the formulations [36]. Atomic absorption spectroscopy was used as complement the TGA data in order to estimate the MNPs composition. The achieved data are listed in Table 3 with those corresponding to TGA.

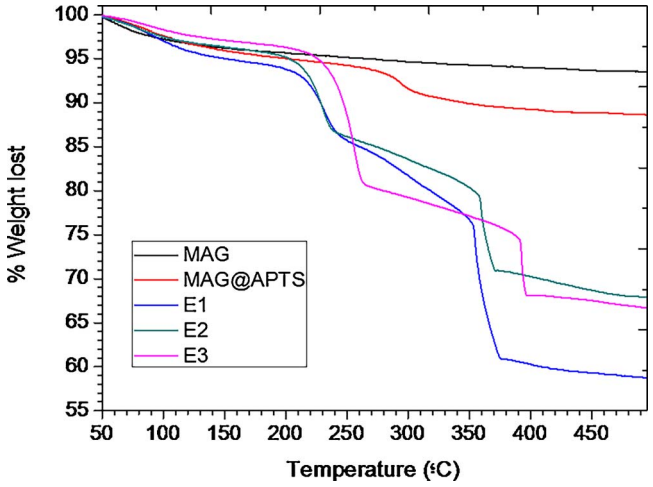

Fig. 4. Thermograms of MAG, MAG@APTS, and samples obtained by covalent linkage of FA on MAG@APTS'surface (E1, E2 and E3).

Table 3
Composition of MNPs estimated from TGA and A.A.

Sample	% Fe_3O_4 (A.A)	%Additives[a] (A.A)	% Additives (TGA)
MAG	78.0 ± 0.52	22.0 ± 0.52	5.0
MAG@APTS	70.0 ± 0.52	30.0 ± 0.52	11.0
E1	46.1 ± 0.17	53.9 ± 0.17	41.0
E2	53.5 ± 0.52	46.6 ± 0.52	33.0
E3	61.1 ± 0.17	38.9 ± 0.17	33.5

[a] Additives include all components excluding magnetic core, i.e: SDS, APTS, FA.

From the results on the table it is possible infer that increasing the FA nominal amount did not reach higher FA incorporated on the MNPs surface. It may assume that a maximum concentration of FA would be admissible on MAG@APTS surface, independently on the nominal amount of FA offered.

An exhaustive characterization of magnetic core, MAG, regarding of its crystalline structure (by XRD) and magnetic properties (by VSM) was

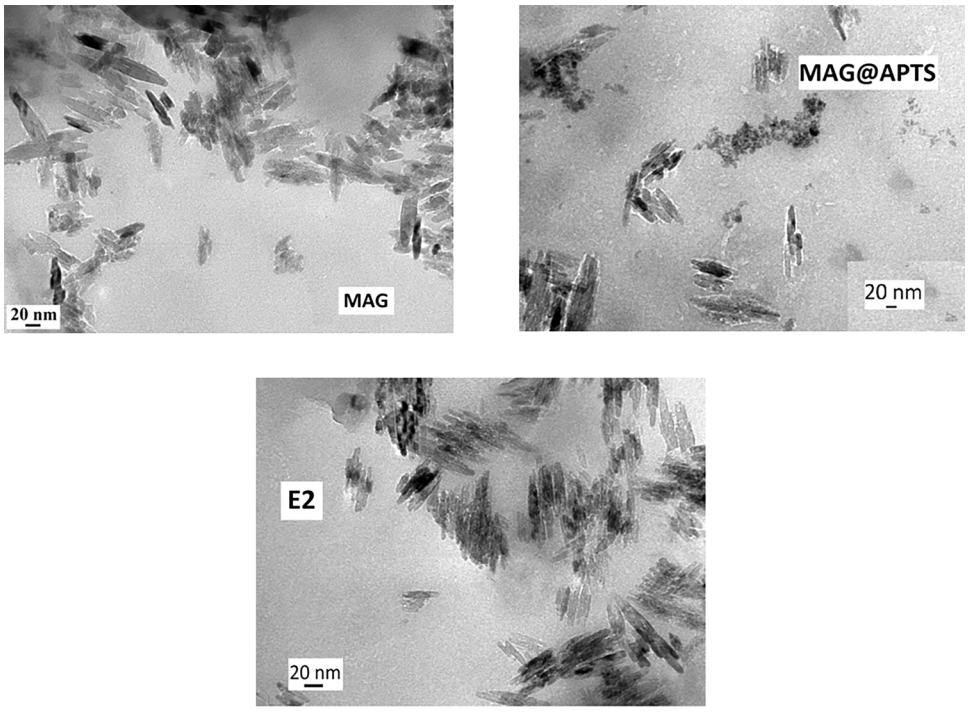

Fig. 3. TEM images of MAG, MAG@APTS and E2.

carried out and reported in own previous work [16].

3.2. Interactions MNPs@FA

The receptor for FA or folate receptor (FR) is highly attractive as target for tumor-specific drug delivery, because of two main reasons: by one side, is overexpressed in several human cancers, including malignancies of the ovary, brain, kidney, breast, myeloid cells and lung. By the other side, FR density may be taken as a parameter to know about the stage/grade of the cancer worsens. An additional correlation has been found between the level of FR and the resistance of certain tumors to chemotherapy [37].

Different ambiguous data have been found in open literature concerning to the FA selective functional groups determining its affinity against FR [38].

After a brief survey of available literature, it emerges that most articles refer to pteridine ring as the sites that bind preferentially to the FR [39]. Whereas the interactions of α or γ carboxyl groups of FA with others molecules generally do not modify the retention of FR affinity [40].

For instance, Li et. al.; immobilized FA on magnetic bovine serum albumin (BSA) microcapsules (FA-MBMCs). FA was immobilized onto the MBMC walls by carboxyl groups bonding with amidogen groups as a targeting ligand to obtain FA-MBMCs. They evaluated the microdevices selectivity employing HeLa cells. The recovered data suggested that the cellular uptake of C6-loaded FA-MBMCs was induced by FA-dependent pathway. Hence the incorporation of FA was crucial to selectively target the tumor cells via FR mediated endocytosis. Indeed, interactions FA-FR were not affected by the coupling of FA thought its carboxyl groups [41].

Aranda et al. prepared nanoparticle systems based on poly(D,L-lactide-*co*-glycolide) acid (PLGA) for delivery of Doxo. In a later step the surface was modified with glutamic acid and FA as targeting ligand. Prior to FA conjugation to PLGA/γ-PGA nanoparticles, the FA was modified with EDA to obtain FA-NH_2, so that there would be certainty that FA was successfully conjugated through the carboxylic acid. With this derivatization the authors ensured that FA retains its ability of binding to folate receptors by specific recognition (pteridine ring) [42].

According to the characterization data it may be inferred that, in present case, the pteridine group has not been compromised in the interactions with MNPs surface functional groups. Therefore, a mechanism involving possible interactions has been elaborated and included in Scheme 2.

Theoretical studies were attained as a complement, to better support the proposed mechanism. Two MNPs coated APTS@FA systems were obtained for reaction between the amino group of the APTS and the carboxyl groups of the FA. As it can be seen in Scheme 2, the geometry (1) is formed when the α carboxyl group of FA reacts with the amino group of the APTS, while the geometry 2 is determined by reaction of APTS with the γ carboxyl group of FA. Relevant energy change (E_{reac}), bond length (d) and OP values belonging to the fully optimized structures are presented in Table inserted in Scheme 2. Results shown that the geometry (1) is slightly more stable (about 6.3 kJ mol^{-1}) than the geometry (2). In fact, the calculated energy change for the APTS + FA → APTS/FA + H_2O process is −27.14 kJ mol^{-1} for the geometry (1) and −20.86 kJ mol^{-1} for the geometry (2). No significant differences were found in the N—C bond length for these two geometries. In the same way, the obtained overlap population (OP) values suggest that the N—C bond belonging to the geometry (1) is only 1.0% stronger than that corresponding to the geometry (2). The theoretical modeling allows inferring that the two analyzed APTS@FA geometries have almost the same stability. These findings strengthen the proposed mechanism revealing that APTS could react with either α or γ FA carboxyl group preserving the reactive site able to bind to FR.

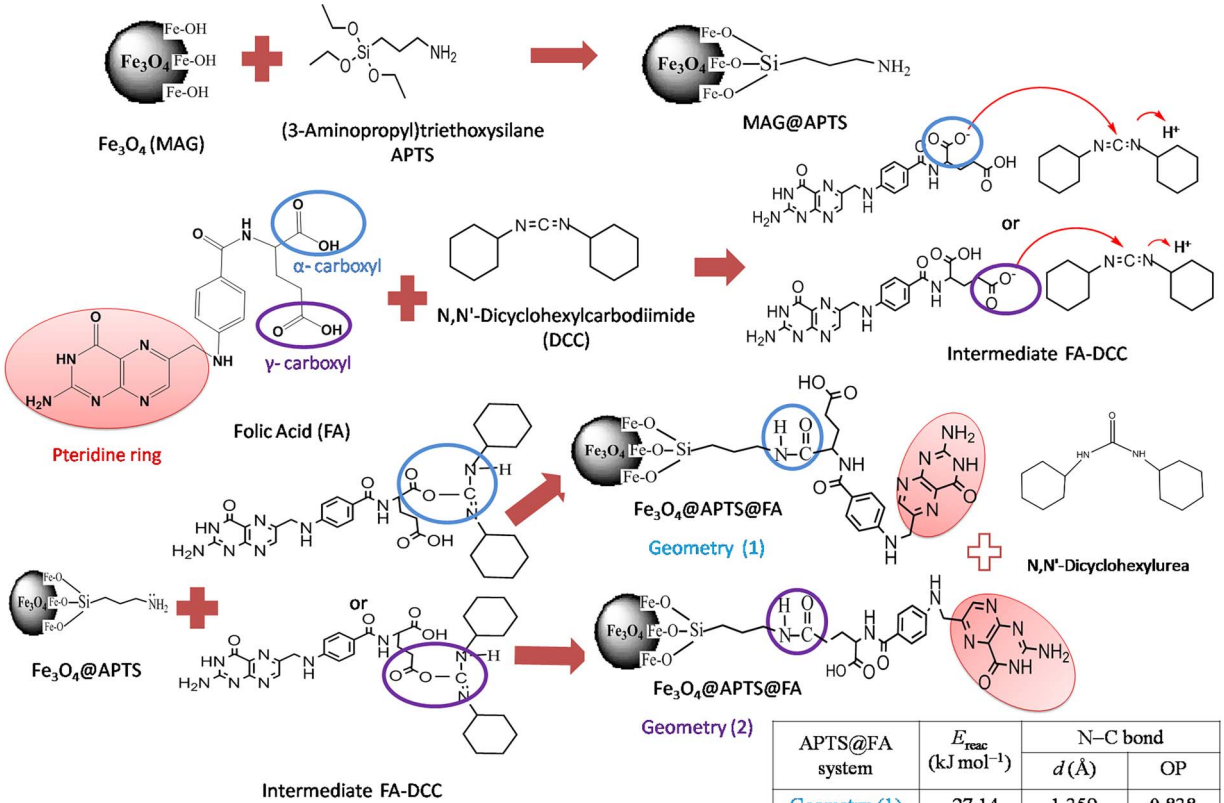

APTS@FA system	E_{reac} (kJ mol^{-1})	N–C bond	
		d (Å)	OP
Geometry (1)	−27.14	1.359	0.838
Geometry (2)	−20.86	1.360	0.829

Scheme 2. Proposed mechanism for possible interactions between MAG@APTS and FA though DCC intermediate reaction.

3.3. Stability of different formulations in terms of the retention of FA on MAG@APTS surface

As it has been demonstrated by characterization data, incorporation of the FA was successfully attained using almost any of the tested incorporation routes. However, a strong requirement associated the loss of FA prior to reach the diana organ, tissue or cell should be considered in view of the practical implementation of these nanodevices.

In general, the literature reports the selectivity to folate-modified nano/microdevices measured in different tumoral cell lines defining variable incubation times (i.e 2, 4, 6, 24 h). For instance, E. Allard-Vannier et al. analysed the uptake of magnetic nanoparticles coated PEG-FA using tumoral cell lines differing in its expression level of FR. To do this they employed HeLa cells having ca. 40-fold higher level of FR than MCF-7 cells while MDA-MB435 cells have no significant FR expression. They found that HeLa cells were characterized by nearly two fold higher uptake of MNPs-FA than MCF-7 cells. In addition, MNPs-FA uptake by MDA-MB435 cells was only slightly lower than that by MCF-7 cells [43]. In this study, the cell culture assays were performed by incubating MNPs in the culture media during 2 h. However, from the exposed results is not possible infer if in such environment, FA remained linked to the MNPs surface or in fact it was released and, in this case, cell cultures were exposed to free FA.

It is worth mention that in most of the reported works these issues are missed [36,44].

FTIR analysis was developed on dried MAG@APTS@FA after incubation in buffer PBS, pH = 7.4 and in distilled water as selected media. The formulation obtained from covalent FA binding appears to be highly stable. In particular, E2 retained the FA almost 4 h in PBS and already 15 days in distilled water (see Supplementary material (b)). The same procedure was followed for E1 and E3, reaching almost similar results than E2 (see Supplementary material (c) and (d)).

From the analysis of the data described above, both E1 and E2 would result suitable for theranostic development regarding to their ability to fix and retain FA under almost physiological conditions. In this concern, E2 was selected to complete the theranostic design by loading the therapeutic agent.

It is worth mention that these issues (stability and interaction mechanism) related to FA containing nanodevices are actually missed in the published articles, as it was earlier stated.

3.4. Analysis on the behaviour of MAG@APTS and E2 on simulated plasmatic media

MNPs were incubated in a media simulating the plasmatic fluids (SPF) in terms of protein content, pH and ionic strength. The evolution of their physicochemical properties in this environment could be taken as a preliminary view regarding their behavior once in vivo administrated. It is well known that physicochemical properties of the MNPs conditioned the feasibility of interactions in physiological media [45]. Once nanosystems are introduced in the biological environment, they are rapidly covered by plasmatic proteins, being human serum albumin (analogous to BSA) the most abundant. This dynamic process ends with the formation of a protein corona around the MNPs surface.

Properties of the MNPs such as size, shape, composition, surface functionality and surface charge are the factor defining the structure and composition of protein corona [46–48].

Fig. 5 shows MAG@APTS and E2 spectra before and after their contact with SPF. In the figure the signals assigned to MAG@APTS and E2, were earlier described, and are clearly visualized. Stretching band around 1650 and 1590 cm^{-1} appears in both spectra, MAG@APTS@BSA and E2@BSA. This band may be ascribed to C=O stretching vibration of amide-I and amide II (N–H bending vibration and the C=N stretching vibration), confirming the presence of α-helix structure of BSA on modified nanoparticles. It is expected since BSA is the main protein present in the SPF [49–51]. The absence of bands around 1000 from the Si–O–Si groups in this spectrum could be also considered as a proof of the interaction of BSA-MAG@APTS. Moreover, in the E2@BSA spectrum some bands of E2 overlap with those corresponding to albumin groups.

Thermal analysis comparing MAG@APTS with MAG@APTS@BSA; and E2 with E2@BSA behavior, further demonstrated the efficient protein incorporation in both formulations from extra mass loss. In the case of MAG@APTS@BSA the mass loss (roughly 14%) was registered at 350 °C, whereas in E2@BSA started at 425 °C reaching 15%. The described thermograms are included in figures (e) and (f) of Supplementary material. Both temperatures of mass loss and% of coated protein are in line with previous work analyzing similar nanosystems [49,52].

Other evidences related to the satisfactory interaction of BSA with E2 are visualized in data recompiled from TEM, hydrodynamic diameter and Z potential measurements. Fig. 6a depicts representative TEM image of E2 after 4 h of treatment with SPF. The figure suggests that nanorods magnetic particles are aggregated in a matrix of BSA. From the image, it is not possible distinguishing whether serum incubation of MNPs leads to a homogeneous layer of proteins on the particle surface or rather to protein bundles containing some MNP. This agrees with other researchers findings [52].

Fig. 6b shows the ζ, for formulations before and after incubation in SPF. As it is seen, interactions with plasmatic protein BSA have a great impact on the MNPs surface charge. In the case of MAG@APTS a high reduction in the ζ, from −8.4 ± 0.7 mV to −19.3 ± 0.4 mV was observed after incubating in SPF. An inverse trend is evidenced in the case of E2 after the same treatment. BSA is an amphoteric protein with isoelectric point at pH = 4.8. According with available literature, surface charge of BSA at pH 7.8 is −18 mV [53,54].The similarity observed in ζ of both formulations (MAG@APTS@BSA and E2@BSA) after incubation in SPF may be attributed to the high number of BSA molecules binding on MNPs surface. These results are consistent with the data achieved by FTIR, and TEM regarding these formulations.

Works reported by other authors devoted to the study of protein corona in nanosystems of diverse surface charge, demonstrated that serum incubation significantly changes the surface charge of particles, and ensured that, independent of the surface charge of particles before incubation, serum-treated particles reveal a negatively charged surface showing a zeta potential lower than −20 mV [52,55,56]. The nature of BSA-MNPs interactions may be associated to conformational changes in the protein structure as a function of pH. Hence, BSA adsorption would be ruled, not only by electrostatic and hydrophobic interactions [54,57], but also by the conformational alteration of its structure in the

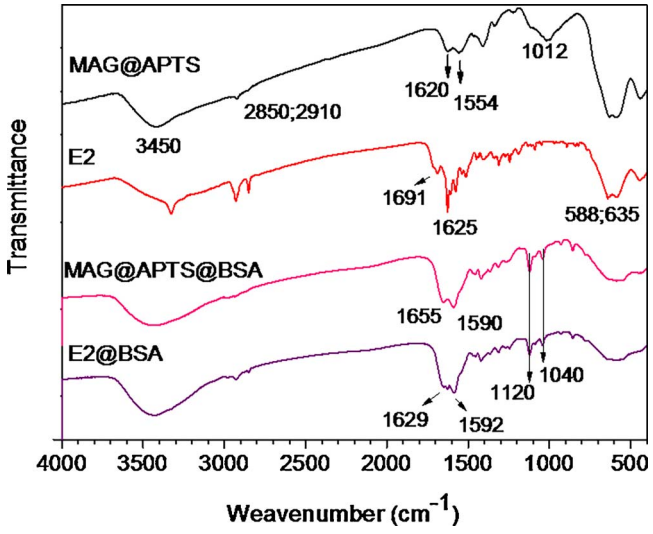

Fig. 5. FTIR spectra of MNPs before and after contact with SPF.

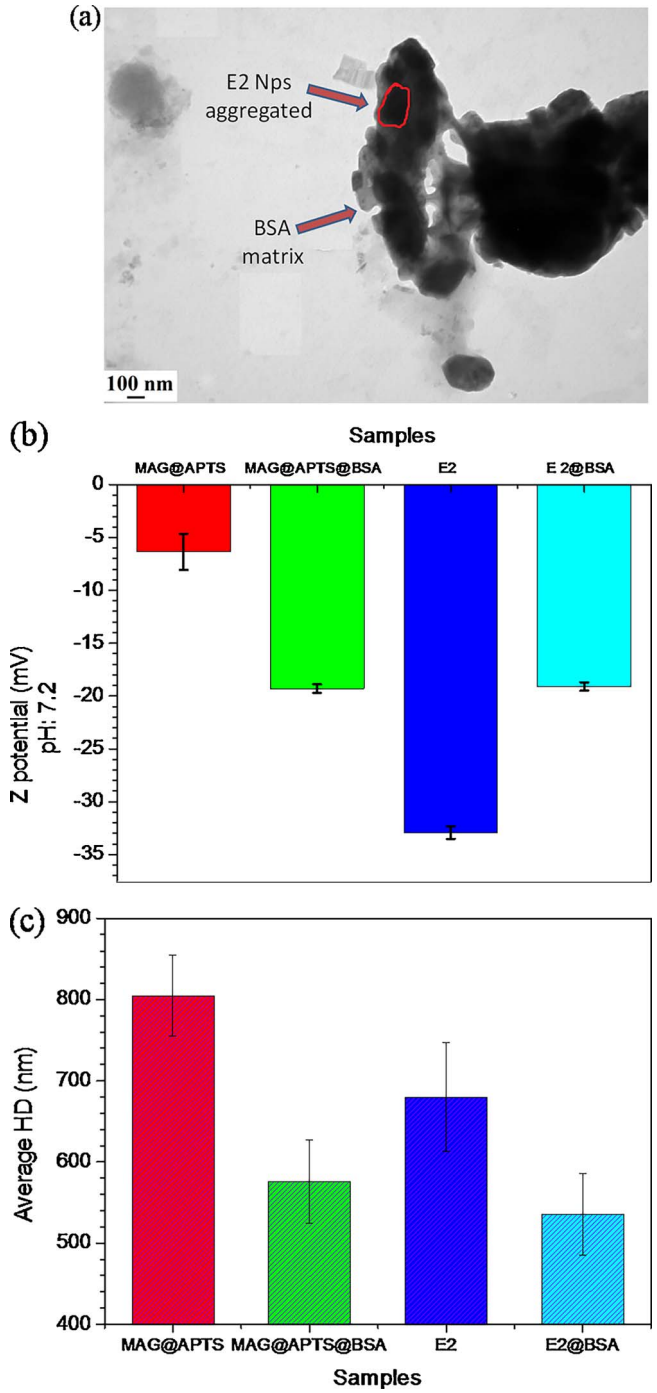

Fig. 6. (a) TEM images of E2 after SPF treatment. (b) Modification of MNPs' ζ in SPF media. (c) Effect of SPF incubation on MNPs HD.

incubation media [58].

Fig. 6c depicts data of HD for raw MNPs and BSA-coated MNPs, both incubated in SPF without protein. From the data it is possible infer that the formation of BSA corona plays a sensitive role over the aggregation trend of MNPs, conferring stability in physiological media [59]. Similar results were found for several authors reporting a reduction in the aggregation by means of serum proteins [46,60].

Other authors have proposed that the protein would form complex with ions from SPF, protecting the MNPs surface by screening these ions from interacting directly with the MNPs surface, thus keeping the MNPs stable in the SPF media [61].

Moreover, the HD evolution as a function of the time was monitored in SPF media without protein and taken as parameter of stability. The data collected using all formulations is included as figure (g) in Supplementary material. This suggests that formulations coated with BSA resulted more stable in SPF than the raw MNPs, at least during 24 h taking as the assay time.

The feasibility of the MNPs-FA to bind BSA represents a promising perspective in view of their in vivo performance, according to published contributions. For instance Sinnecker et al. reported in vitro experiments using Caco-2 cells and intestinal epithelial cells, concluding that pre-treatment of nanoparticles (NPs) with BSA reduced the adherence of the NPs to the cells by enhancing the NPs colloidal stability and alleviating adherence [62]. Gonzalez Moragas et al. proposed that, BSA-coated NPs interact less with biological environments than their non-coated counterparts. In view of this result, BSA-coated NPs could travel within an organism to reach specific tissues efficiently (quickly) and harmlessly (with low unspecific interactions) [55].

3.5. Incorporation of therapeutic agent: doxorubicin

E2 was treated with Doxorubicin to provide the therapeutic function to assess magnetic theranostics. A preliminary verification of the Doxo incorporation on E2 surface was given for changes in the dispersion color. While the raw E2 (MNPs-FA) dispersion was slightly brown, a red coloration appeared after Doxo adsorption (see Fig. 7a). Such coloration persisted even after drying the nanoparticles.

FTIR spectroscopy was employed to verify the satisfactory incorporation of Doxo on E2 surface. Spectra of raw Doxo, E2@Doxo and E2 are compared in Fig. 7b. In Fig. 7c the region about 1200–850 cm^{-1} of E2 and E2@Doxo spectra is expanded in order to better appreciate the bands related to the drug. From the analysis of these figures, it is observed a shift of the band assigned to υ(C—O), from 1070 cm^{-1} to 1017 cm^{-1} in the spectra of raw drug and E2@Doxo, respectively. Besides, the signal associated to υ(C—O—C), shifted from 997 cm^{-1} to 989 cm^{-1} in Doxo spectrum and E2@Doxo respectively [63]. These findings confirmed the successful drug incorporation, through probably, electrostatic attraction and hydrogen bonding [13].

It is important to highlight that this assay constitutes a preliminary one, since only a specific condition was employed in terms of experimental conditions selected to assess the Doxo incorporation. Such conditions were taken from previous works using other therapeutic agents [33,34].

4. Concluding remarks

Novel insight concerning the preparation of magnetic nanotheranostics was provided.

The incorporation of FA to the MNPs surface as target ligand was optimized, finding the most suitable binding route not only from the loaded FA point of view, but also mainly on the stability and retention of MNPs physicochemical properties.

Characterization data revealed that both vias, adsorption and covalent binding, ensured satisfactory FA loadings in nanocarriers. However, covalent linkage using intermediate FA concentration was the most suitable route in terms of the ligand retention on the MNPs structure.

Mechanism of interaction MNPs@FA was elucidated using experimental data derived from characterization. Such data was corroborated by theoretical calculations. From this data, it was confirmed that the pteridine group remained available to target FR, demonstrating the potential of this theranostic to detect, for instance, circulating tumor cells.

The behavior of MNPs@FA in simulated physiological media revealed that the physicochemical properties of MNPs remained almost invariable while a satisfactory interaction with BSA was evidenced. In this context, it is expected that the nanosystems result suitable for in vivo administration.

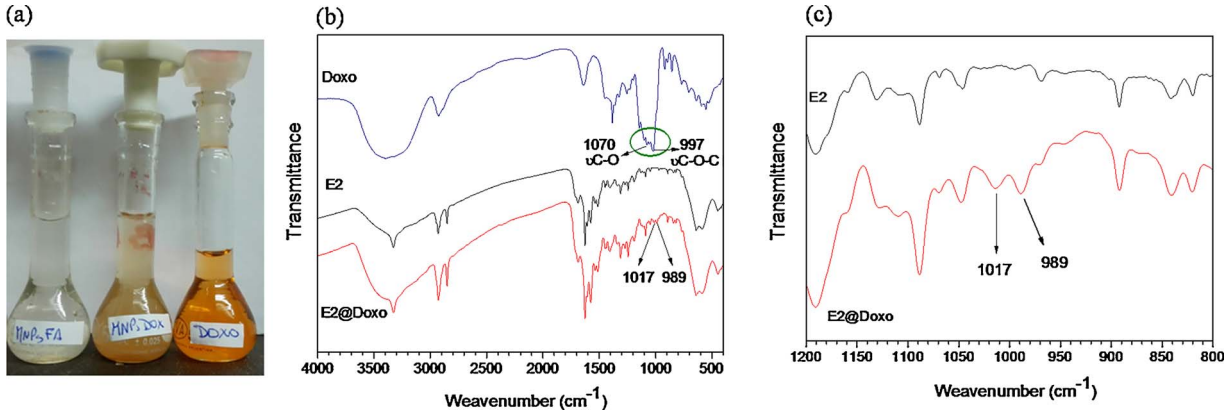

Fig. 7. (a) Photographs of MNPs dispersions and Doxo solution in water. (b) FTIR spectra of pure Doxo E2 and E2@Doxo. (c) Magnification of figure b in the region between 1200 and 850 cm^{-1}.

Finally, the ability to loading an oncological drug such as Doxorubicin was verified though FTIR spectroscopy. Currently an in deep study exploring a range of Doxo concentrations, analysing the adsorption kinetic and the encapsulation of the drug is in development. The data achieved from this work will take part of a separate report.

Acknowledgements

The authors acknowledge Dra. Ma. Fernanda Horst, INQUISUR (UNS/CONICET) for assistance with Atomic absorption spectroscopy measurements, the financial support of CONICET, ANPCyT (PICT 2013 1984) and UNS (PGI24/ZQ09). I.L.C. and V.L. are members of CONICET. P.A. is CONICET fellowship.

Appendix A. Supplementary data

Supplementary data associated with this article can be found, in the online version, at http://dx.doi.org/10.1016/j.colsurfa.2017.10.025.

References

[1] H. Hashemi-Moghaddam, S. Kazemi-Bagsangani, M. Jamili, S. Zavareh, Evaluation of magnetic nanoparticles coated by 5-fluorouracil imprinted polymer for controlled drug delivery in mouse breast cancer model, Int. J. Pharm. 497 (2016) 228–238.
[2] S. Kelkar, T. Reineke, Theranostics: combining imaging and therapy, Bioconjugate Chem. 22 (2011) 1879–1903.
[3] R. Jurado, P. Frączek, M. Droetto, P. Sánchez, E. Valero, J.M. Domínguez-Vera, N. Gálvez, Apomaghemite as a doxorubicin carrier for anticancer drug delivery, J. Inorg. Biochem. 157 (2016) 46–51.
[4] K. Kim, J.H. Kim, H. Park, Yoo-Shin Kim, K. Park, H. Nam, S. Lee, J.H. Park, Rang-Woon Park, In-San Kim, K. Choia, S.Y. Kime, Tumor-homing multifunctional nanoparticles for cancer theragnosis: simultaneous diagnosis, drug delivery, and therapeutic monitoring, J. Control. Release 146 (2010) 219–227.
[5] P. Dadras, F. Atyabi, S. Irani, L. Mamani, A. Foroumadi, Z. Hadavand Mirzaie, M. Ebrahimi, R. Dinarvand, Formulation and evaluation of targeted nanoparticles for breast cancer theranostic system, Eur. J. Pharm. Sc. 97 (2017) 47–54.
[6] M. Thakur, A. Mewada, S. Pandey, M. Bhori, K. Singh, M. Sharon, M. Sharon, Milk-derived multi-fluorescent graphene quantum dot-based cancer theranostic system, Mater. Sci. Eng. C 67 (2016) 468–477.
[7] L.R. Jaidev, D. Raj Chellappan, D. Vasanth Bhavsar, R. Ranganathan, B. Sivanantham, A. Subramanian, U. Sharma, N.R. Jagannathan, U. Maheswari Krishnan, S. Sethuraman, Multi-functional nanoparticles as theranostic agents for the treatment & imaging of pancreatic cancer, Acta Biomater. 49 (2017) 422–433.
[8] T.T.-D. Tran, P.H.-L. Tran, T.-J. Yoon, B.-J. Lee, Fattigation-platform theranostic nanoparticles for cancer therapy, Mater. Sci. Eng. C 75 (2017) 1161–1167.
[9] A. Pourjavadi, S. Hassan Hosseini, M. Alizadeh, C. Bennett, Magnetic pH-responsive nanocarrier with long spacer length and high colloidal stability for controlled delivery of doxorubicin, Colloids Surf. B 116 (2014) 49–54.
[10] M. Angelakeris, Magnetic nanoparticles: a multifunctional vehicle for modern theranostics, Biochim. Biophys. Acta 1861 (2017) 1642–1651.
[11] R. Jin, B. Lin, D. Li, H. Ai, Superparamagnetic iron oxide nanoparticles for MR imaging and therapy: design considerations and clinical applications, Curr. Opin. Pharmacol. 18 (2014) 18–27.
[12] Z. Wanga, C. Zhou, J. Xia, B. Via, Y. Xia, F. Zhang, Y. Li, L. Xia, Fabrication and characterization of a triple functionalization of graphene oxide with Fe_3O_4, folic acid and doxorubicin as dual-targeted drug nanocarrier, Colloids Surf. B 106 (2013) 60–65.
[13] Y. Huang, K. Mao, B. Zhang, Y. Zhao, Superparamagnetic iron oxide nanoparticles conjugated with folic acid for dual target-specific drug delivery and MRI in cancer theranostics, Mater. Sci. Eng. C 70 (2017) 763–771.
[14] S.-J. Yang, F.-H. Lin, K.-C. Tsai, M.-F. Wei, H.-M. Tsai, J.-M. Wong, M.-J. Shieh, Folic acid-conjugated chitosan nanoparticles enhanced protoporphyrin IX accumulation in colorectal cancer cells, Bioconjugate Chem. 21 (2010) 679–689.
[15] K. Patel, B.S. Raj, Y. Chen, X. Lou, Novel folic acid conjugated Fe_3O_4-ZnO hybrid nanoparticles for targeted photodynamic therapy, Colloids Surf. B 150 (2017) 317–325.
[16] P. Azcona, R. Zysler, V. Lassalle, Simple and novel strategies to achieve shape and size control of magnetite nanoparticles intended for biomedical applications, Colloids Surf. A 504 (2016) 320–330.
[17] Q.L. Jiang, S.W. Zheng, R.Y. Hong, S.M. Deng, L. Guo, R.L. Hu, B. Gao, M. Huang, L.F. Cheng, G.H. Liu, Y.Q. Wang, Folic acid-conjugated Fe_3O_4 magnetic nanoparticles for hyperthermiaand MRI in vitro and in vivo, Appl. Surf. Sci. 307 (2014) 224–233.
[18] Y.Y. He, X.C. Wang, P.K. Jin, B. Zhao, X. Fan, Complexation of anthracene with folic acid studied by FTIR and UV spectroscopies, Spectrochim. Acta Mol. Biomol. Spectrosc. 72 (2009) 876–879.
[19] P. Ordejón, E. Artacho, J.M. Soler, Self-consistent order-N density-functional calculations for very large systems, Phys. Rev. B 53 (1996) R10441–4.
[20] J.M. Soler, E. Artacho, J.D. Gale, A. García, J. Junquera, P. Ordejón, The SIESTA method for ab initio order-N materials simulation, J. Phys.: Condes. Matter. 14 (2002) 2745–2779.
[21] J.P. Perdew, K. Burke, M. Ernzerhof, Generalized gradient approximation made simple, Phys. Rev. Lett. 77 (1996) 3865–3868.
[22] J. Junquera, O. Paz, D. Sánchez-Portal, E. Artacho, Numerical atomic orbitals for linear-scaling calculations, Phys. Rev. B 64 (2001) 235111.
[23] N. Troullier, J.L. Martins, Efficient pseudopotentials for plane-wave calculations, Phys. Rev. B 43 (1991) 1993–2006.
[24] R. Hoffmann, Solids and surfaces, A Chemist's View of Bonding in Extended Structures, VCH Publ. Inc., New York, 1988.
[25] S. Sadighiana, K. Rostamizadeh, H. Hosseini-Monfareda, M. Hamidi, Doxorubicin-conjugated core-shell magnetite nanoparticles asdual-targeting carriers for anticancer drug delivery, Colloids Surf. B 117 (2014) 406–413.
[26] Y.Y. Hea, X.C. Wang, P.K. Jin, B. Zhao, X. Fan, Complexation of anthracene with folic acid studied by FTIR and UV spectroscopies, Spectrochim. Acta Mol. Biomol. Spectrosc. 72 (2009) 876–879.
[27] K. Can, M. Ozmen, M. Ersoz, Immobilization of albumin on aminosilane modified superparamagnetic magnetite nanoparticles and its characterization, Colloids Surf. B 71 (2009) 154–159.
[28] M. Ma, Y. Zhang, W. Yu, H.-ying Shen, H.-qian Zhang, N. Gu, Preparation and characterization of magnetite nanoparticles coated by amino silane, Colloids Surf. A 212 (2003) 219–226.
[29] C. Weigel, R. Kellner, FTIR-ATR-spectroscopic investigation of the silanization of germanium surfaces with 3-aminopropyltriethoxysilane, Z. Anal. Chem. 335 (1989) 663–668.
[30] H. Cao, J. He, L. Deng, X. Gao, Fabrication of cyclodextrin-functionalized superparamagnetic Fe_3O_4/amino-silane core-shell nanoparticles via layer-by-layer method, Appl. Surf. Sci 255 (2009) 7974–7980.
[31] J. Zhang, S. Rana, R.S. Srivastava, R.D.K. Misra, On the chemical synthesis and drug delivery response of folate receptor-activated: polyethylene glycol-functionalized magnetite nanoparticles, Acta Biomater. 4 (2008) 40–48.
[32] M.F. Cabrerizo, G. Petroselli, C. Lorente, A.L. Capparelli, A.H. Thomas, A.M. Braun, E. Oliveros, Substituent effects on the photophysical properties of pterin derivatives in acidic and alkaline aqueous solutions, Photochem. Photobiol. 81 (2005) 1234–1240.
[33] M. Agotegaray, A. Campelo, R. Zysler, F. Gumilar, C. Bras, A. Minetti, V. Massheimer, V. Lassalle, Influence of chitosan coating on magnetic nanoparticles in endothelial cells and acute tissue biodistribution, J. Biomater. Sci. Polym. Ed. 27

(2016) 1069–1085.
[34] M. Agotegaray, A. Campelo, R. Zysler, F. Gumilar, C. Bras, A. Gandini, A. Minetti, V. Massheimer, V. Lassalle, Magnetic nanoparticles for drug targeting: from design to insights into systemic toxicity. Preclinical evaluation of hematological, vascular and neurobehavioral toxicology, Biomater. Sci. 5 (2017) 772–783.
[35] H. Li, Z. Li, J. Zhao, B. Tang, Y. Chen, Y. Hu, Z. He, Y. Wangfalta, Carboxymethyl chitosan-folic acid-conjugated Fe_3O_4@SiO_2 as a safe and targeting antitumor nanovehicle in vitro, Nanoscale Res. Lett. 9 (2014) 146–157.
[36] X. Feng, S. Zhang, H. Wu, X. Lou, A novel folic acid-conjugated TiO_2-SiO_2 photosensitizer for cancer targeting in photodynamic therapy, Colloids Surf. B 125 (2015) 197–205.
[37] G. Toffoli, A. Russo, A. Gallo, C. Cernigoi, S. Miotti, R. Sorio, S. Tumolo, M. Boiocchi, Expression of folate binding protein as a prognostic factor for response to platinum-containing chemotherapy and survival in human ovarian cancer, Int. J. Cancer 79 (1998) 121–126.
[38] M. Hansen, E. Greibe, S. Skovbjerg, S. Rohde, A. Kristensen, T. Jensen, C. Stentoft, K. Kjær, C. Kronborg, P. Martensen, Folic acid mediates activation of the pro-oncogene STAT3 via the Folate Receptor alpha, Cell. Signal. 27 (2015) 1356–1368.
[39] Y. Lu, P. Low, Folate-mediated delivery of macromolecular anticancer therapeutic agents, Adv. Drug Deliv. Rev. 64 (2012) 342–352.
[40] C.P. Leamon, R.B. DePrince, R.W. Hendren, Folate-mediated drug delivery: effect of alternative conjugation chemistry, J. Drug Target. 7 (1999) 157–169.
[41] Z. Li, S. Liu, S. Wang, L. Qiang, T. Yang, H. Wang, H. Möhwald, X. Cui, Synthesis of folic acid functionalized redox-responsive magnetic proteinous microcapsules for targeted drug delivery, J. Colloid Interface Sci. 450 (2015) 325–331.
[42] L. Aranda-Lara, G. Ferro-Flores, F.M. de Ramírez, B. Ocampo-García, C. Santos-Cuevas, L. Díaz-Nieto, K. Isaac-Olivé, Improved radiopharmaceutical based on 99mTc-Bombesin-folate for breast tumour imaging, Nucl. Med. Commun. 37 (2016) 377–386.
[43] K. E.Allard-Vannier, K. Hervé-Aubert, T.t Kaaki, A. Blondy, K. Shebanova, A. Shaitan, M.-L. Ignatova, A. Saboungi, I. Feofanov, Chourpa Folic acid-capped PEGylated magnetic nanoparticles enter cancer cells mostly via clathrin dependent endocytosis, Biochim. Biophys. Acta 2016 (1861) 1578–1586.
[44] L.T.T. Huong, N.H. Nam, D.H. Doan, H.T.M. Nhung, B.T. Quang, P.H. Nam, P.Q. Thong, N.X. Phuc, H.P. Thu, Folate attached, curcumin loaded Fe_3O_4 nanoparticles: a novel multifunctional drug delivery system for cancer treatment, Mater. Chem. Phys. 172 (2016) 98–104.
[45] V. Forest, J. Pourchez, Preferential binding of positive nanoparticles on cell membranes is due to electrostatic interactions: a too simplistic explanation that does not take into account the nanoparticle protein corona, Mater. Sci. Eng. C 70 (2017) 889–896.
[46] E. Izak-Nau, M. Voetz, S. Eiden, A. Duschl, V.F. Puntes, Altered characteristics of silica nanoparticles in bovine and human serum: the importance of nanomaterial characterization prior to its toxicological evaluation, Part. Fibre Toxicol. 10 (2013) 56.
[47] N.P. Mortensen, G.B. Hurst, W. Wang, C.M. Foster, P.D. Nallathamby, S.T. Retterer, Dynamic development of the protein corona on silica nanoparticles: composition and role in toxicity, Nanoscale 5 (2013) 6372–6380.
[48] E. Brun, C. Sicard-Roselli, Could nanoparticle corona characterization help for biological consequence prediction, Cancer Nanotechnol. 5 (2014) 7–20.
[49] S.K. Swain, D. Sarkar, Study of BSA protein adsorption/release on hydroxyapatite nanoparticles, Appl. Surf. Sci. 286 (2013) 99–103.
[50] A.K. Bordbar, A.A. Rastegari, R. Amiri, E. Ranjbakhsh, M. Abbasi, A.R. Khosropour, Characterization of modified magnetite nanoparticles for albumin immobilization, Biotechnol. Res. Int. 2014 (2014) 6, http://dx.doi.org/10.1155/2014/705068 Article ID 705068.
[51] B. Zhang, H. Zhang, X. Li, X. Lei, C. Li, D. Yin, X. Fan, Q. Zhang, Synthesis of BSA/Fe_3O_4 magnetic composite microspheres for adsorption of antibiotics, Mater. Sci. Eng. C 33 (2013) 4401–4408.
[52] A. Weidner, C. Gräfe, H. von der Lühe, D. Clement, F. Eberbeck, R. Müller, F.H. Schacher, S. Dutz, Preparation of core-shell hybrid materials by producing a protein corona around magnetic nanoparticles, Nanoscale Res. Lett. 10 (2015) 282–293.
[53] T.J. Peters, Serum albumin, Adv. Protein Chem. 37 (1985) 161–245.
[54] J. Gonzalez, P. Nicolas, M.L. Ferreira, M. Avena, V. Lassalle, V. Alvarez, Fabrication of ferrogels using different magnetic nanoparticles and their performance on protein adsorption, Polym. Int. 63 (2014) 258–265.
[55] L. Gonzalez-Moragas, S.-M. Yu, E. Carenza, A. Laromaine, A. Roig, Protective effects of bovine serum albumin on superparamagnetic iron oxide nanoparticles evaluated in the nematode caenorhabditis elegans, Biomater. Sci. Eng. 1 (2015) 1129–1138.
[56] M. Lundqvist, J. Stigler, G. Elia, I. Lynch, T. Cedervall, Kenneth A. Dawson, Nanoparticle size and surface properties determine the protein corona with possible implications for biological impacts, Proc. Natl. Acad. Sci. U. S. A. 105 (2008) 14265–14270.
[57] Z.G. Peng, K. Hidajat, M.S. Uddin, Adsorption of bovine serum albumin on nanosized magnetic particles, J. Colloid Interface Sci. 271 (2004) 277–283.
[58] B.D. Fair, A.M. Jamieson, Studies of protein adsorption on polystyrene latex surfaces, J. Colloid Interface Sci. 77 (1980) 525–534.
[59] D. Eberbeck, M. Kettering, C. Bergemann, P. Zirpel, I. Hilger, L. Trahms, Quantification of the aggregation of magnetic nanoparticles with different polymeric coatings in cell culture medium, J. Phys. D: Appl. Phys. 43 (2010) 405002–405011.
[60] A.C. Sabuncu, J. Grubbs, S. Qian, T.M. Abdel-Fattah, M.W. Stacey, A. Beskok, Probing nanoparticle interactions in cell culture media, Colloids Surf. B 95 (2012) 96–102.
[61] S.-M. Yu, L. Gonzalez-Moragas, M. Milla, A. Kolovou, R. Santarella-Mellwig, Y. Schwab, A. Laromaine, A. Roig, Bio-identity and fate of albumin-coated SPIONs evaluated in cells and by the C elegans model, Acta Biomater. 43 (2016) 348–357.
[62] H. Sinnecker, K. Ramaker, A. Frey, Coating with luminal gutconstituents alters adherence of nanoparticles to intestinal epithelial cells, Beilstein J. Nanotechnol. 5 (2014) 2308–2315.
[63] S. Kayal, R.V. Ramanujan, Doxorubicin loaded PVA coated iron oxide nanoparticles for targeted drug delivery, Mater. Sci. Eng. C 30 (2010) 484–490.